

Room-temperature photoluminescence of Mg-doped GaN thin films grown by plasma-assisted MOCVD

Cite as: AIP Advances 10, 045123 (2020); <https://doi.org/10.1063/5.0004384>

Submitted: 10 February 2020 . Accepted: 31 March 2020 . Published Online: 17 April 2020

Pepen Arifin, Sugiarto, Agus Subagio, Heri Sutanto , Donny Dwiputra, Fenfen F. Florena, Aveni C. Keintjem, and Rany Khaeroni



View Online



Export Citation



CrossMark



NEW

AVS Quantum Science

A new interdisciplinary home for impactful quantum science research and reviews

Co-Published by



NOW ONLINE

Room-temperature photoluminescence of Mg-doped GaN thin films grown by plasma-assisted MOCVD

Cite as: AIP Advances 10, 045123 (2020); doi: 10.1063/5.0004384

Submitted: 10 February 2020 • Accepted: 31 March 2020 •

Published Online: 17 April 2020



Pepen Arifin,^{1,a)} Sugianto,² Agus Subagio,³ Heri Sutanto,³  Donny Dwiputra,¹ Fenfen F. Florena,¹ Aveni C. Keintjem,¹ and Rany Khaeroni¹

AFFILIATIONS

¹Physics of Electronic Materials Division, Department of Physics, Faculty of Mathematics and Natural Sciences (FMIPA), Institute of Technology Bandung (ITB), Jl. Ganesha 10, Bandung 40132, Indonesia

²Department of Physics, State University of Semarang, Sekaran, Gunungpati, Semarang 50229, Indonesia

³Department of Physics, University of Diponegoro, Jl. Prof. Soedharto, SH, Tembalang, Semarang 50275, Indonesia

^{a)} Author to whom correspondence should be addressed: pepen@fi.itb.ac.id

ABSTRACT

The growth of Mg-doped GaN thin films by metalorganic chemical vapor deposition (MOCVD) using NH_3 and Cp_2Mg as a source of nitrogen and Mg, respectively, usually produces Mg–H complexes, which hinder the activation of Mg as shallow acceptor centers. Therefore, post-growth treatments are commonly required to activate these acceptor centers. The presence of Mg dopants in GaN films induces various defect-related emissions whose characteristics depend on the growth method. For this study, we prepared Mg-doped GaN thin films by plasma-assisted MOCVD. A nitrogen-plasma, instead of NH_3 , served as a nitrogen source to minimize the formation of Mg–H complexes, thereby eliminating the requirement for post-growth treatment. The emission characteristics were obtained by measuring the photoluminescence of the as-grown room-temperature films. Yellow, green, blue, and ultraviolet emission bands are produced by Mg-doped samples with different Mg concentrations produced by Cp_2Mg flow rates of 2%, 5%, and 10% of the total flow rate. Low-Mg concentration leads to nitrogen and gallium vacancies, which results in yellow photoluminescence. At higher Mg concentration, the yellow photoluminescence is suppressed and the blue photoluminescence is enhanced because of the incorporation of vacancies by Mg atoms. The analysis of the photoluminescence spectra leads to the proposed band diagrams for Mg-doped GaN with varying Mg concentration.

© 2020 Author(s). All article content, except where otherwise noted, is licensed under a Creative Commons Attribution (CC BY) license (<http://creativecommons.org/licenses/by/4.0/>). <https://doi.org/10.1063/5.0004384>

I. INTRODUCTION

Due to their superior optical properties, the group III-nitrides have played a major role in optoelectronic device applications, such as LEDs, laser diodes, solid-state lighting, and solar-blind ultraviolet detectors.^{1–4} Remarkable progress in the development of optoelectronic devices has been made since the synthesis of *p*-type GaN. Various dopants, such as Zn, Be, or Mg, have been used; however, Mg is the most important dopant because it leads to reproducible *p*-type GaN.⁵ Growing Mg-doped GaN by metalorganic chemical vapor deposition (MOCVD) produces a high-resistivity material with low hole concentration that prevents it from being used

for high-efficiency LEDs or laser diodes that operate at low voltage. These characteristics are caused by Mg–H complexes that form during the film's growth through the decomposition of NH_3 and Cp_2Mg .^{6–8} Therefore, additional treatments are required to activate Mg as a shallow acceptor. Several post-growth treatments have been tested, such as rapid thermal annealing, low-energy electron-beam irradiation, and photo-enhanced activation.^{9–11}

Various defect-related emissions are commonly present in GaN films. In *n*-type unintentionally doped GaN or lightly doped GaN, yellow luminescence (YL) usually appears as a broad band that peaks at ~ 2.2 eV. The origin of the YL band has been a controversy for some years; however, it is now widely accepted that it is

related to gallium-vacancy-related defects (V_{Ga}) or carbon-related defects.¹² MOCVD-grown Mg-doped GaN occasionally produces a green luminescence (GL) band that peaks around 2.4–2.5 eV. This emission is related to Mg-dopant-associated defects caused by nitrogen vacancies.¹³ Finally, the most common emission bands in Mg-doped GaN are a blue luminescence (BL) band that peaks around 2.9 eV and an ultraviolet luminescence (UVL) band that peaks around 3.2 eV. The BL band commonly appears in heavily Mg-doped MOCVD-grown GaN. The BL band is attributed to transitions from deep donors, formed by hydrogen defects, to shallow Mg_{Ga} acceptors.^{5,14,15} The deep-donor level involved with the BL band is about 0.4 eV below the conduction band and is sometimes attributed to the $V_{\text{N}}\text{Mg}_{\text{Ga}}$ complex.⁵ The UVL band involves electronic transitions from the conduction band to Mg_{Ga} acceptors.^{5,16}

In MOCVD-grown GaN, the Mg–H complex produces defect-related emission, so a method of fabricating GaN that avoids the formation of the Mg–H complex would be preferred. Plasma-assisted MOCVD may be such an alternative method for growing GaN and its alloys. This growth technique uses the nitrogen plasma, instead of NH_3 , as a source of nitrogen and can be used to grow III-nitrides with minimal formation of Mg–H complexes. In addition, the growth temperature is lower than that of thermal MOCVD.^{17,18} Thus, Mg-doped GaN grown by plasma-assisted MOCVD should not require post-treatment to activate the Mg dopants.

The nitrogen plasma is generated primarily by electron cyclotron resonance (ECR) microwave sources and radio frequency sources. All such sources produce a nitrogen species consisting of a mixture of neutral molecular, charged molecular, ionic, and neutral atomic nitrogen species, together with free electrons.¹⁹ However, each source produces different proportions of nitrogen species, which influences the growth mechanism. An understanding of the nitrogen species generated by the plasma source is thus essential to produce high-quality GaN films. For this purpose, different radio frequency and ECR plasma sources have received intensive studies.^{20–24}

The goal of developing a nitrogen plasma source is to generate reactive nitrogen species with a higher concentration of neutral nitrogen species than highly energetic ionic nitrogen species. The latter species is avoided because it may damage the film surface.^{22,25} This type of reactive nitrogen species that reacts with gallium determines the growth mechanism, which, in turn, affects the properties of the films grown. For example, the highly energetic ionic nitrogen species gives rise to Ga vacancies (V_{Ga}),²⁶ which are responsible for the formation of a deep acceptor level. In contrast, the growing GaN film under a Ga-rich atmosphere produces a high concentration of N vacancies (V_{N}), which are responsible for the formation of shallow donor levels.²⁷

In this paper, we report the room-temperature photoluminescence characteristics of plasma-assisted MOCVD-grown Mg-doped GaN films. Instead of using NH_3 as a nitrogen source, as commonly done in thermal MOCVD, plasma-assisted MOCVD growth uses reactive nitrogen species produced by the ECR plasma from pure nitrogen gas. The use of reactive nitrogen species should minimize the formation of Mg–H defect complexes during growth, which would eliminate the requirement for post-growth treatment to activate Mg as a shallow acceptor. Optimized growth conditions were used to produce high-quality GaN films, and we observed pho-

toluminescence in various bands, depending on the Mg concentration. The characteristics of the observed photoluminescence are correlated with the growth mechanism.

II. EXPERIMENT

Mg-doped GaN films were grown on (0001) sapphire substrates by plasma-assisted MOCVD. Trimethylgallium and bis-cyclopentadienyl magnesium (Cp_2Mg) were used as Ga and Mg sources, respectively, and the reactive nitrogen plasma served as a nitrogen source. The nitrogen plasma was produced by a low-power downstream plasma generator installed inside the reactor. The growth method and mechanism were similar to that described by Arifin *et al.*²⁸ Three samples of Mg-doped GaN films were grown with flow rates of Cp_2Mg of 2%, 5%, and 10% of the total flow rate, while the flow rates of trimethylgallium and N_2 gas were maintained at 0.08 SCCM and 90 SCCM, respectively. The growth processes lasted 2 h, with the result being ~0.5- μm -thick Mg-doped GaN films. Hydrogen plasma treatment was not used during growth to avoid the formation of Mg–H bonds.

Photoluminescence (PL) measurements were made at room temperature by using a Kimmon He–Cd laser at 325 nm as an excitation source. The PL emission was detected by using a photomultiplier and analyzed by using a SPEX-1000 monochromator. A notch filter of 325 nm was used to prevent any laser light from entering the photomultiplier detector. The PL measurement setup used the lock-in technique to improve the signal-to-noise ratio. The structural properties of the grown layers were characterized by x-ray diffraction (XRD) using the Cu K α line (1.546 Å), and the electrical properties were measured by using the Hall–van der Pauw method.

III. RESULTS AND DISCUSSION

Figure 1 shows the XRD spectra of Mg-doped GaN thin films grown at 650 °C with Cp_2Mg flow rates of 2%, 5%, and 10%. All films exhibit a single-crystal structure with a strong orientation along the *c* axis of the hexagonal structure. No other diffraction peaks with comparable intensities appear. The 2θ diffraction angles are 34.60° and 73.05°, which correspond to the (0002) and (0004) planes of GaN, respectively. This indicates that the film is epitaxially crystallized despite a large lattice mismatch between GaN and the sapphire substrate. The presence of the GaN buffer layer is believed to reduce the lattice-mismatch effect.

Figure 2 shows the room-temperature PL spectra of the as-grown GaN samples doped with Cp_2Mg flow rates of 2% (MG2), 5% (MG5), and 10% (MG10). The samples have hole concentrations of $2.97 \times 10^{17} \text{ cm}^{-3}$, $9.35 \times 10^{17} \text{ cm}^{-3}$, and $1.14 \times 10^{19} \text{ cm}^{-3}$, respectively, as measured by using the Hall–van der Pauw method. With no post-growth treatment, all samples emit PL features at various energies. Samples MG2 and MG5 exhibit the strongest PL line above 3.4 eV (not shown). Both samples emit a UVL peak: sample MG2 at 3.23 eV and sample MG5 at 3.27 eV. The shift in the UVL peak of around 0.04 eV is attributed to the increase in Mg concentration and is consistent with the observations of Ogino *et al.*²⁹ The MG5 sample emits BL over a broad band that peaks at 2.8 eV and 2.91 eV and a YL band that peaks at 2.2 eV. The MG5 sample also emits a GL band that peaks near 2.5 eV, which is consistent with

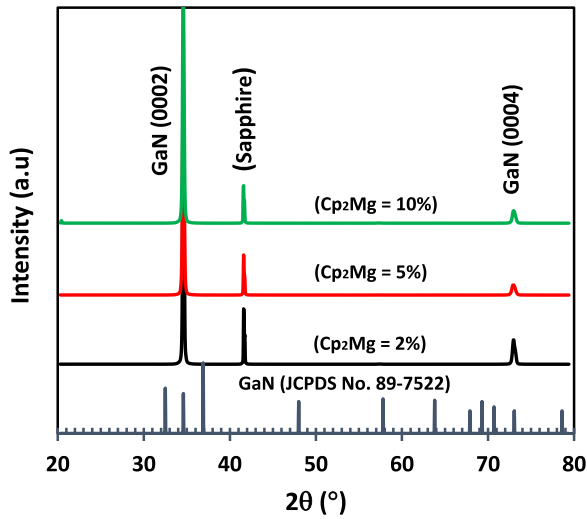


FIG. 1. XRD spectra of Mg-doped GaN thin films grown at 650 °C with Cp₂Mg flow rates of 2%, 5%, and 10%. The diffraction peaks are assigned to the hexagonal phase and correspond to the (0002) and (0004) planes of wurtzite GaN (JCPDS card, No. 89-7522).

the previous research.^{5,30,31} Interestingly, when the Cp₂Mg flow is increased to 10% (sample MG10), the YL and GL bands disappear and the PL spectrum becomes dominated by a broader BL band, with a strongly diminished UVL band peaking at 3.23 eV still apparent. These results reveal that increasing the concentration of the Mg dopant strengthens the BL band and suppresses the YL band.

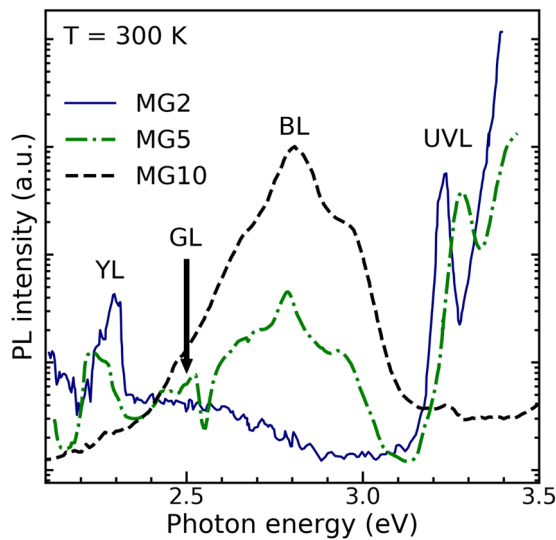


FIG. 2. PL spectra of plasma-assisted MOCVD-grown Mg-doped GaN with Cp₂Mg flow rates of 2% (MG2), 5% (MG5), and 10% (MG10) of the total flow rate.

We now analyze the PL spectra of samples MG5 and MG10 to resolve the YL, GL, and BL bands. The spectral peaks and profiles of the YL, GL, and BL bands as well as the PL intensity $I^{PL}(E)$ are fit with the following formula derived from the one-dimensional configuration-coordinate model:^{13,32}

$$I^{PL}(E) = I_{\max}^{PL} \exp \left[-2S_e \left(\sqrt{\frac{E_0^* - E}{E_0^* - E_{\max}}} - 1 \right)^2 \right]. \quad (1)$$

The band is characterized by a maximum PL intensity I_{\max}^{PL} , the Huang–Rhys factor is denoted by S_e , and the band peak energy is denoted by E_{\max} . The denominator under the radical is the Stokes shift, with $E_0^* = E_0 + 0.5\hbar\Omega$, where E_0 is the zero-phonon line and $\hbar\Omega$ is the energy of the effective phonon mode corresponding to the excited state.³³ Figures 3 and 4 show the fitted curves. The difference between the PL spectra and the curve fit given by Eq. (1) is mainly attributed to the low-temperature assumption involved in the derivation of Eq. (1)^{13,32} (recall that these spectra were measured at room temperature). Equation (1) is thus useful to resolve the peaks and their corresponding parameters, but the zero-phonon line is essentially indistinguishable in the room-temperature spectra. Table I gives the parameter values obtained from fitting to the YL, GL, and BL bands.

Figure 3 shows the normalized PL spectrum of the MG5 sample at around the YL and GL bands and their curve fits. The intensity of the YL peak at 2.24 eV exceeds that of the GL band. A further increase in Mg concentration (i.e., to that of sample MG10) reduces the intensity of the YL band, whereas the BL band becomes prominent. Although the intensity of the YL band at a low temperature is usually not prominent,^{13,32} we detect a notably strong intensity of the

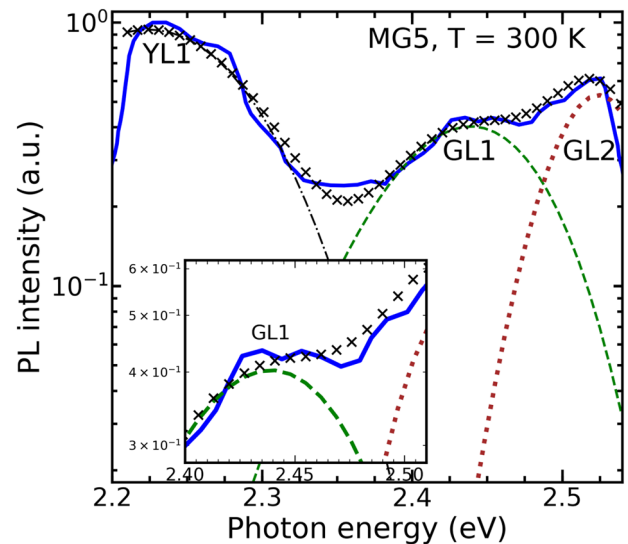


FIG. 3. Normalized PL spectra showing YL and GL bands of the MG5 sample. The inset shows an expanded view of the spectrum near the peak of band GL1. The dashed-dotted, dashed, and dotted lines are fits of Eq. (1) to the YL1, GL1, and GL2 bands, respectively. The crosses (x) show the sum of the calculated intensities of the YL1, GL1, and GL2 bands.

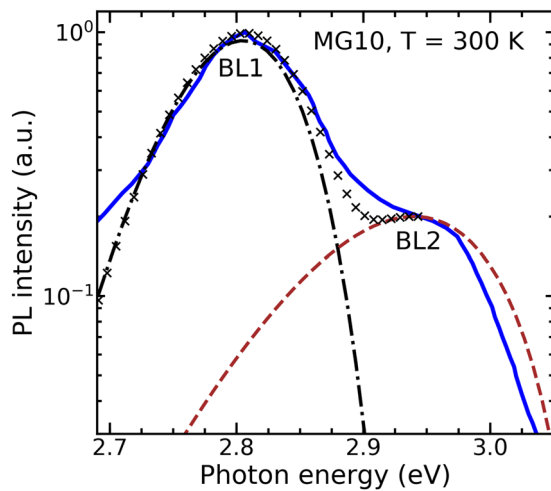


FIG. 4. Normalized PL spectra showing BL bands of the MG10 sample. The dashed-dotted and dashed lines are fits of Eq. (1) to the BL1 and BL2 bands, respectively. The crosses (x) show the sum of the calculated BL1 and BL2 bands.

YL peak. This result for lightly Mg-doped GaN thin films is similar to that of the work of Ramaiah *et al.*³⁰ As the temperature increases to 300 K, the intensity of the YL band continues to increase above that of the BL band. In the case of Mg-doped c-GaN films, YL emission is also observed at 300 K.³⁴

Figure 4 shows a normalized PL spectrum of the BL bands of the MG10 sample and the associated fits. The fitted PL intensity of the BL band has two peaks: a stronger peak at 2.80 eV and a weaker peak at 2.94 eV. The transition energies of the GL and BL bands are 2.52 eV, 2.80 eV, and 2.94 eV and are strongly consistent with the results of previous research.³⁵ For example, Jeong *et al.* reported the PL spectra of Mg-doped GaN thin films grown by MOCVD and annealed in a N₂ atmosphere at 900 °C for 30 s to activate the hydrogen-passivated Mg acceptors. The spectra are dominated by the BL band with a peak of 2.8 eV, which, when fit with multiple Gaussians, gives peaks at 2.548 eV, 2.760 eV, and 2.898 eV. These energies are interpreted as the transition energies between deep donors and shallow Mg acceptors located at 0.22 eV above the valence band.³⁵

Based on the fitted parameter E_{\max} for the YL, GL, and BL bands, we deduce the energy levels within the electronic bandgap to reproduce the various transition levels; Fig. 5 shows the result. The dashed double-ended arrows show the energy differences between

TABLE I. Parameter values from fitting Eq. (1) to YL, GL, and BL bands.

Band	I_{\max}^{PL}	S_e	E_0^* (eV)	E_{\max} (eV)
YL1	0.94	36.9	2.62	2.224
GL1	0.403	20.4	3.67	2.439
GL2	0.53	47.8	2.72	2.524
BL1	0.93	9.8	2.95	2.805
BL2	0.2	3.6	3.08	2.940

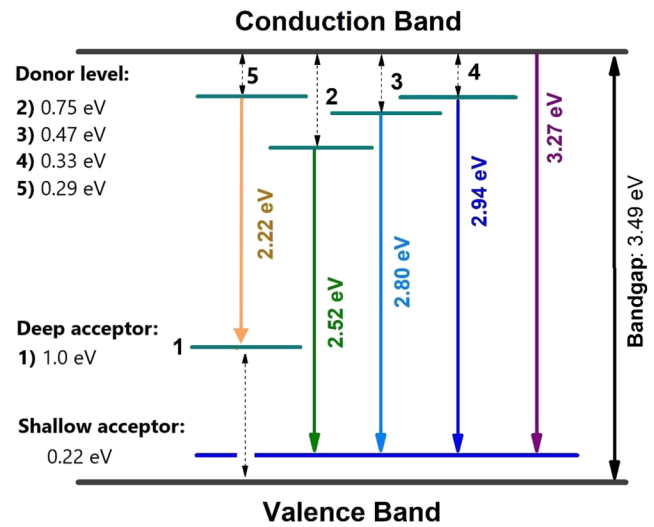


FIG. 5. Proposed donor and acceptor energy levels and the recombination processes involved in plasma-assisted MOCVD-grown Mg-doped GaN.

the acceptor and the donor levels and the respective band edge, and the single-headed arrows show the transition energy. We use a bandgap energy of 3.49 eV obtained from transmission spectroscopy measurements of undoped GaN and the commonly accepted Mg shallow acceptor level of 0.22 eV above the valence band.³⁶ For otherwise-undoped GaN with a low concentration of the Mg dopant, YL is always present and is commonly associated with point defects of isolated nitrogen and gallium vacancies.^{5,13} Two models have been proposed to explain the YL within the framework of the donor-acceptor pair-recombination mechanism, which involves transitions between a shallow donor and a deep acceptor^{37,38} or between a deep donor and a shallow acceptor.³⁹ Determining which mechanism produces YL requires an understanding of the growth process. The growth of GaN using plasma-assisted MOCVD uses a highly energetic nitrogen plasma. In our case, the nitrogen plasma is dominated by the excited states of neutral N₂^{*} molecules, with no ionic nitrogen or atomic nitrogen observed.²⁸ Bombardment by highly energetic neutral N₂^{*} gives rise to Ga vacancies, which are responsible for the deep acceptor level,²⁶ which is predicted to be around 1.0 eV above the valence band, although it varies from sample to sample.⁴⁰

The growth of GaN via plasma-assisted MOCVD also uses a very high V/III ratio of around 1100. A consequence of this is a higher fraction of nitrogen, which causes nitrogen vacancies. These nitrogen vacancies are associated with the shallow donor level that makes undoped GaN an *n*-type material. In our routine procedure for growing undoped GaN, *n*-type GaN is always obtained. The shallow donor level is due to the incorporation of carbon and oxygen atoms in the gallium and nitrogen vacancies, as predicted by the *ab initio* local-density-functional method.⁴¹ Thus, YL in GaN is more likely due to the transition between the shallow donor level and the deep acceptor level. By subtracting the YL peak energy (2.2 eV) and the deep acceptor energy of 1.0 eV (with respect to the valence band) from the bandgap of 3.49 eV, we obtain the shallow donor level at 0.29 eV below the conduction band.

The Mg dopant substitutes into the Ga vacancy (Mg_{Ga}), thereby forming the Mg shallow acceptor level at 0.22 eV above the valence band. The process involves diffusion of Mg_i to Ga vacancy sites to give substitutional Mg at Ga sites.⁴² The existence of the shallow acceptor level is responsible for the UVL (3.27 eV), which is produced by the transition from the conduction band to the shallow acceptor level. However, the substitution of Mg into Ga vacancies (V_{Ga}) means that increasing the Mg concentration should decrease the Ga vacancy concentration and, consequently, decrease the YL. The results of PL measurements confirm that the YL intensity decreases with increasing Mg concentration.

The YL band thus decreases as the Mg concentration increases, whereas new broad and dominant emission appears in the blue region, with peaks at 2.8 eV and 2.94 eV. The blue emissions are associated with donor-acceptor pair transitions and are also affected by Mg doping of GaN. At higher Mg concentration (i.e., sample MG10), insufficient Ga vacancies are available so that Mg_i must diffuse to V_{Ga} sites and are thereby converted to Mg_{Ga} . Alternatively, given their relatively low formation energy, the Mg_i adatoms may combine with other suitable defects to form defect complexes such as $Mg_{Ga} + Mg_i$. This defect complex promotes the formation of a deep donor state in the bandgap,⁴³ as per the hybrid HSE06-functional-based calculation, the donor levels due to the $Mg_{Ga} + Mg_i$ and Mg_i defects are 3.14 eV and 3.07 eV above the valence band.⁴³ For the present case, the BL band transition energies are 2.94 eV and 2.80 eV, which, given the Mg shallow acceptor level at 0.22 eV above the valence band, places the donor levels at 3.16 eV and 3.02 eV above the valence band or at 0.33 eV and 0.47 eV below the conduction band, respectively. These results are strongly consistent with those obtained by Nayak *et al.*⁴³ Thus, the BL peaks at 2.94 eV and 2.80 eV are due to transitions between deep donor levels at 0.33 eV and 0.47 eV below the conduction band, respectively, and shallow acceptor levels at 0.22 eV above the valence band. Consequently, an increase in Mg concentration suppresses YL because of the lack of Mg incorporation into Ga vacancies.

Two possible transitions may explain the energy of the GL band that peaks at 2.52 eV: a transition from the conduction band to a deep acceptor level of around 0.9–1.0 eV and a transition from a deep donor level to a shallow acceptor level.¹³ However, given that the GL band is present in moderately doped GaN (i.e., MG5) whereas no GL band appears in either low-doped GaN (i.e., MG2) or highly doped GaN (i.e., MG10), the GL band should not be related to the deep acceptor level. Otherwise, the YL band and the GL band should both be emitted by lightly doped GaN (i.e., MG2). Because the formation of Mg_{Ga} involves the diffusion of Mg_i to Ga vacancies, the concentration of Mg_i depends simultaneously on the concentration of V_{Ga} and Mg dopants. At low Mg concentration, V_{Ga} concentration is high and most Mg dopants diffuse to V_{Ga} sites to form Mg_{Ga} . At moderate Mg concentration, a fraction of Mg cannot find a V_{Ga} site and produces Mg_i defects, which may produce the deep donor level, which is similar to the mechanism reported by Nayak *et al.*⁴³ except that the donor-level energy depends on the concentration of Mg_i . By subtracting the transition energy of the GL band (2.52 eV) and the Mg acceptor level of 0.22 eV (with respect to the valence band) from the bandgap energy, we obtain a donor level 0.75 eV below the conduction band.

To further investigate the proposed model of donor and acceptor energy levels and the recombination processes in Mg-doped GaN grown by plasma-assisted MOCVD, we study the correlation between Mg incorporation into the GaN matrix during the growth process and the defects formed therein. Mg incorporation into the GaN matrix causes doping-induced strain that can be detected by monitoring the angle and width of the peaks in the XRD spectra. Toward this end, Fig. 6 plots the XRD peaks around $2\theta = 34.6^\circ$ to determine the full width at half maximum (FWHM) as a function of Cp_2Mg flow rate. The FWHM of the XRD peak correlates with lattice strain or crystallite size. The average crystallite size D can be estimated by using the following Debye-Scherrer formula:

$$D = \frac{0.9\lambda}{\beta \cos \theta}, \quad (2)$$

where λ is the x-ray wavelength (1.546 Å), β is the FWHM, and θ is the Bragg diffraction angle. The calculated average crystallite size is presented in Table II, and the respective bandgaps of Mg-doped GaN were obtained from UV-vis spectroscopy (data not shown). Since the average crystallite size is much greater than the Bohr radius of the GaN exciton (2.8 nm),⁴⁴ therefore, the crystallite size does not much influence on the bandgap. However, the bandgap is influenced by the doping density.

At room temperature, we assume that the hole concentration is the same as the doping density. Increasing the doping density decreases the bandgap because of an increased overlap of the wave functions of electrons bound to the impurity atoms. The change in bandgap energy as a function of doping density is given by

$$\Delta E_g(N) = -\frac{3e^3}{16\pi\epsilon_s} \sqrt{\frac{N}{\epsilon_s k_B T}}, \quad (3)$$

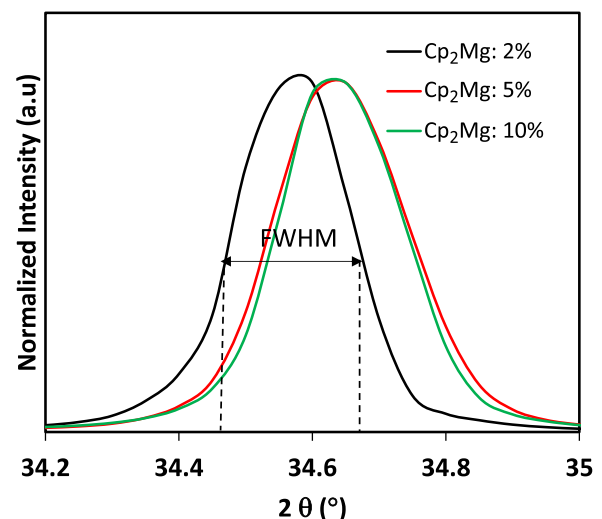


FIG. 6. Normalized XRD spectra of Mg-doped GaN with various Cp_2Mg flow rates (2%, 5%, and 10% of the total flow rate for samples MG2, MG5, and MG10, respectively). The diffraction peaks of samples MG5 and MG10 are shifted to a higher angle, indicating an increase in the lattice constant.

TABLE II. Estimated crystallite size and bandgap of GaN thin films grown at various Cp₂Mg flow rates (given as percent of total flow rate).

Cp ₂ Mg flow rate (%)	Hole concentration (cm ⁻³)	FWHM (deg)	Crystallite size (nm)	Bandgap ^a (eV)	Bandgap ^b (eV)
2 (MG2)	2.97×10^{17}	0.225	37.1	3.42	3.47
5 (MG5)	9.35×10^{17}	0.24	34.8	3.40	3.45
10 (MG10)	1.14×10^{19}	0.22	37.9	3.36	3.37

^aCalculated from UV-vis spectroscopy.^bCalculated by using Eq. (3).

where N is the doping density, e is the fundamental charge, ϵ_s is the dielectric constant of the semiconductor, k_B is the Boltzmann constant, and T is the absolute temperature. For the hole concentrations given in Table I, the calculated values for ΔE_g are -19 meV, -34 meV, and -118 meV. Given that the bandgap of undoped GaN is 3.49 eV, the estimated bandgaps are 3.47 eV, 3.45 eV, and 3.37 eV for samples MG2, MG5, and MG10, respectively.

The growth of Mg-doped GaN by plasma-assisted MOCVD is commonly done with a high V/III ratio. At low doping concentration (sample MG2), the growth process leads to deep acceptor, shallow acceptor, and shallow donor levels due to the formation of V_{Ga} , Mg_{Ga} , and V_N , respectively. Because magnesium has an atomic radius slightly greater than that of gallium and much greater than that of nitrogen, the tensile and compressive strains due to the presence of V_N , V_{Ga} , and Mg_{Ga} should compensate each other, resulting in strain relaxation, which is confirmed by the relatively small FWHM of the XRD peak. Moreover, the presence of Mg_{Ga} causes the bandgap to shrink to 3.42 eV. At the greater Mg concentration of sample MG5, insufficient Ga vacancies are available, so Mg_i diffuses to V_{Ga} sites and converts to Mg_{Ga} , with some Mg_i remaining. The remaining Mg_i induces compressive strain that increases the lattice constant, which is detected by the shift of the XRD peaks to a larger angle 2θ . Concurrently, the increased Mg concentration results in a further decrease in the bandgap to 3.40 eV. Further increasing the Mg concentration to that of sample MG10 results in the formation of Mg_i and $Mg_{Ga} + Mg_i$ defects, which should decrease the bandgap and further increase the compressive strain, thereby increasing the FWHM of the XRD peak. However, although the bandgap shrinks as expected, the FWHM of the XRD peak decreases to that of sample MG2. The decrease in the FWHM upon increasing the doping concentration from MG5 to MG10 indicates that the strain in sample MG10 has relaxed to the same level as that in sample MG2, which has a low dopant concentration. Because the Mg concentration is, indeed, greater in sample MG10 than in sample MG2, the relaxation of strain may be tentatively attributed to an increase in bending dislocations and tensile strain, as observed by Soman *et al.* and Prinz *et al.*^{45,46}

IV. CONCLUSION

We report the growth of Mg-doped GaN films by plasma-assisted MOCVD with three different Cp₂Mg concentrations. At low Mg concentration, the samples emit yellow and ultraviolet photoluminescence bands with intensities that decrease with increasing

Mg concentration. The yellow photoluminescence is attributed to the transition between shallow donor levels and deep acceptor levels, which are produced by nitrogen and gallium vacancies, respectively. The ultraviolet luminescence is attributed to transitions between the conduction band and shallow acceptor levels created by Mg_{Ga} point defects. Increasing the Mg concentration reduces the availability of Ga vacancies, which increases the concentration of Mg_i and $Mg_{Ga} + Mg_i$ defects in the GaN films. These defects are believed to produce the deep donor levels that are responsible for the green and blue luminescence bands.

ACKNOWLEDGMENTS

The authors acknowledge financial support from the Directorate General for Higher Education, The Ministry of National Education, The Republic of Indonesia and from the Research and Community Services Council (LPPM), Institute of Technology Bandung.

The data that support the findings of this study are available from the corresponding author upon reasonable request.

REFERENCES

- H. Amano, *Prog. Cryst. Growth Charact. Mater.* **62**, 126 (2016).
- M. Murayama, Y. Nakayama, K. Yamazaki, Y. Hoshina, H. Watanabe, N. Fuutagawa, H. Kawanishi, T. Uemura, and H. Narui, *Phys. Status Solidi A* **215**, 1700513 (2018).
- S. Pimpitkar, J. S. Speck, S. P. DenBaars, and S. Nakamura, *Nat. Photonics* **3**, 180 (2009).
- S. K. Zhang, W. B. Wang, F. Yun, L. He, H. Morkoç, X. Zhou, M. Tamargo, and R. R. Alfano, *Appl. Phys. Lett.* **81**, 4628 (2002).
- M. A. Reshchikov and H. Morkoç, *J. Appl. Phys.* **97**, 061301-1 (2005).
- S. Nakamura, N. Iwasa, M. Senoh, and T. Mukai, *Jpn. J. Appl. Phys., Part 1* **31**, 1258 (1992).
- M. S. Brant, N. M. Johnson, R. J. Molnar, R. Singh, and T. D. Moustakas, *Appl. Phys. Lett.* **64**, 2264 (1994).
- W. Götz, N. M. Johnson, D. P. Bour, M. D. McCluskey, and E. E. Haller, *Appl. Phys. Lett.* **69**, 3725 (1996).
- S. Nakamura, T. Mukai, M. Senoh, and N. Iwasa, *Jpn. J. Appl. Phys., Part 2* **31**, L139 (1992).
- H. Amano, M. Kito, K. Hiramatsu, and I. Akasaki, *Jpn. J. Appl. Phys., Part 2* **28**, L2112 (1989).
- Y. Kamiura, Y. Yamashita, and S. Nakamura, *Jpn. J. Appl. Phys.*, **37**, L970 (1998).
- M. Julkarnain, N. Kamata, T. Fukuda, and Y. Arakawa, *Opt. Mater.* **60**, 481 (2016).

- ¹³M. A. Reshchikov, D. O. Demchenko, J. D. McNamara, S. Fernandez-Garrido, and R. Calarco, *Phys. Rev. B* **90**, 035207 (2014).
- ¹⁴B. Monemar, P. P. Paskov, G. Pozina, C. Hemmingsson, J. P. Bergman, S. Khromov, V. N. Izyumskaya, V. Avrutin, X. Li, H. Morkoç, H. Amano, M. Iwaya, and I. Akasaki, *J. Appl. Phys.* **115**, 053507 (2014).
- ¹⁵Y. Kamiura, M. Kaneshiro, J. Tamura, T. Ishiyama, Y. Yamashita, T. Mitani, and T. Mukai, *Jpn. J. Appl. Phys., Part 2* **44**, L926 (2005).
- ¹⁶U. Kaufmann, M. Kunzer, H. Obloh, M. Maier, Ch. Manz, A. Ramakrishnan, and B. Santic, *Phys. Rev. B* **59**, 5561 (1999).
- ¹⁷Y. Xu, B. Gu, and F.-W. Qin, *J. Vac. Sci. Technol., A* **22**, 302 (2004).
- ¹⁸S. Fu, J. Chen, H. Zhang, C. Guo, W. Li, and W. Zhao, *J. Cryst. Growth* **311**, 3325 (2009).
- ¹⁹A. V. Blant, O. H. Hughes, T. S. Cheng, S. V. Novikov, and C. T. Foxon, *Plasma Sources Sci. Technol.* **9**, 12 (2000).
- ²⁰W. C. Hughes, W. H. Rowland, Jr., M. A. L. Johnson, S. Fujita, J. W. Cook, Jr., J. F. Schetzina, J. Ren, and J. A. Edmond, *J. Vac. Sci. Technol., B* **13**, 1571 (1995).
- ²¹R. P. Vaudo, J. W. Cook, and J. F. Schetzina, *J. Cryst. Growth* **138**, 430 (1994).
- ²²A. Ohtani, K. S. Stevens, M. Kinniburgh, and R. Beresford, *J. Cryst. Growth* **150**, 902 (1995).
- ²³Z. Y. Fan and N. Newman, *J. Vac. Sci. Technol., A* **16**, 2132 (1998).
- ²⁴A. J. Ptak, M. R. Millecchia, T. H. Myers, K. S. Ziemer, and C. D. Stinespring, *Appl. Phys. Lett.* **74**, 3836 (1999).
- ²⁵T. C. Fu, N. Newman, E. Jones, J. S. Chan, X. Liu, M. D. Rubin, N. W. Cheung, and E. R. Weber, *J. Electron. Mater.* **24**, 249 (1995).
- ²⁶R. J. Molnar and T. D. Moustakas, *J. Appl. Phys.* **76**, 4587 (1994).
- ²⁷P. Boguslawski, E. L. Briggs, and J. Bernholc, *Phys. Rev. B* **51**, 17255 (1995).
- ²⁸P. Arifin, H. Sutanto, A. Subagio, Sugianto, and M. A. Mustajab, *AIP Adv.* **9**, 115304 (2019).
- ²⁹T. Ogino and M. Aoki, *Jpn. J. Appl. Phys.* **19**(12), 2395 (1980).
- ³⁰K. S. Ramaiah, Y. K. Su, S. J. Chang, F. S. Juang, and C. H. Chen, *J. Cryst. Growth* **220**, 405 (2000).
- ³¹B. Z. Qu, Q. S. Zhu, X. H. Sun, S. K. Wan, Z. G. Wang, H. Nagai, Y. Kawaguchi, K. Hiramatsu, and N. Sawaki, *J. Vac. Sci. Technol., A* **21**, 838 (2003).
- ³²M. A. Reshchikov, D. O. Demchenko, A. Usikov, H. Helava, and Y. Makarov, *Phys. Rev. B* **90**, 235203 (2014).
- ³³A. Alkauskas, J. L. Lyons, D. Steiauf, and C. G. Van de Walle, *Phys. Rev. Lett.* **109**, 267401 (2012).
- ³⁴H. Vilchis and V. M. Sánchez-R, *Mater. Sci. Semicond. Process.* **37**, 68 (2015).
- ³⁵T. S. Jeong, J. H. Kim, M. S. Han, K. Y. Lim, C. J. Youn, J. O. Kim, Y. J. Jung, and H. Lee, *J. Cryst. Growth* **280**, 401 (2005).
- ³⁶H. Morkoc, *Handbook of Nitride Semiconductors and Devices*, Electronic and Optical Processes in Nitrides Vol. 2 (Wiley-VCH Verlag GmbH & Co KGaA, Weinheim, 2008), p. 733.
- ³⁷T. L. Tansley and R. J. Egan, *Phys. Rev. B* **45**, 10942 (1992).
- ³⁸P. Perlin, T. Suski, M. Leszczynski, and H. Teisseyre, in *GaN and Related Materials*, edited by S. Pearton (Gordon and Breach Publishers, London, 1997), p. 315.
- ³⁹E. R. Glaser, T. A. Kennedy, K. Doverspike, L. B. Rowland, D. K. Gaskill, J. A. Freitas, Jr., M. Asif Khan, D. T. Olson, J. N. Kuznia, and D. K. Wickenden, *Phys. Rev. B* **51**, 13326 (1995).
- ⁴⁰J. Neugebauer and C. G. Van de Walle, *Phys. Rev. B* **50**, 8067(R) (1994).
- ⁴¹J. Kang, Y. Shen, and Z. Wang, *Mat. Sci. Eng.: B* **91-92**, 303 (2002).
- ⁴²U. Wahl, L. M. Amorim, V. Augustyns, A. Costa, E. David-Bosne, T. A. L. Lima, G. Lippertz, J. G. Correia, M. R. da Silva, M. J. Kappers, K. Temst, A. Vantomme, and L. M. C. Pereira, *Phys. Rev. Lett.* **118**, 095501 (2017).
- ⁴³S. Nayak, M. Gupta, U. V. Waghmare, and S. M. Shivaprasad, *Phys. Rev. Appl.* **11**, 014027 (2019).
- ⁴⁴P. Ramvall, S. Tanaka, S. Nomura, P. Riblet, and Y. Aoyagi, *Appl. Phys. Lett.* **73**, 1104 (1998).
- ⁴⁵R. Soman, N. Mohan, H. Chandrasekar, N. Bhat, and S. Raghavan, *J. Appl. Phys.* **124**, 245104 (2018).
- ⁴⁶G. M. Prinz, M. Feneberg, M. Schirra, R. Sauer, K. Thonke, S. B. Thapa, and F. Scholz, *Phys. Status Solidi RRL* **2**, 215–217 (2008).